Removal of scatter radiation in paediatric cardiac catheterisation

Gould, R., McFadden, S. L., Sands, A. J., McCrossan, B. A., Horn, S., Prise, K. M., Doyle, P., & Mary Hughes, C. (2017). Removal of scatter radiation in paediatric cardiac catheterisation: a randomised controlled clinical trial. *Journal of radiological protection*. https://doi.org/10.1088/1361-6498/aa80a4

Published in:
Journal of radiological protection

Document Version:
Peer reviewed version

Queen's University Belfast - Research Portal:
Link to publication record in Queen's University Belfast Research Portal

Title

Removal of scatter radiation in paediatric cardiac catheterisation: a randomised controlled clinical trial.

Richard Gould PhD[1], Sonyia L. McFadden PhD[1], Andrew J Sands MPhil[2], Brian A. McCrossan MD[2], Simon Horn PhD[3], Kevin M. Prise PhD[3] Philip Doyle PhD[4] and Ciara M. Hughes PhD[1*]

[1] Institute of Nursing and Health Research, Ulster University, Jordanstown Campus, Shore Road, Newtownabbey.

[2] Royal Belfast Hospital for Sick Children, 274 Grosvenor Road, Belfast.

[3] Centre for Cancer Research and Cell Biology, Queens University Belfast, 97 Lisburn Road, Belfast.

[4] Regional Medical Physics Service, Belfast Health and Social Care Trust, Foster Green Hospital, 110 Saintfield Road, Belfast.

[*]Corresponding author:

Ciara Hughes, Institute of Nursing and Health Research, Ulster University, Jordanstown Campus, Shore Road, Newtownabbey, BT37 OQB, United Kingdom.

Email cm.hughes@email.ulster.ac.uk

Keywords: Paediatric cardiac catheterisation, risk of ionising radiation, stochastic effects, radiation dose optimisation DNA double-strand breakage.

Abstract

Objective: This study sought to determine if DNA integrity was compromised by ionising radiation from paediatric cardiac catheterisations and if dose optimisation techniques allowed DNA integrity to be maintained.

Materials and Methods: Children were imaged using either: (i) an anti-scatter grid (current departmental protocol), (ii) no anti-scatter grid or, (iii) no anti-scatter grid and a 15 cm air-gap between the child and the X-ray detector. Dose area product and image quality were assessed, lifetime attributable cancer risk estimates were calculated and DNA double-strand breakages quantified using the γH2AX assay.

Results: Consent was obtained from 70 parents/guardians/children. Image quality was sufficient for each procedure performed. Removal of the anti-scatter grid resulted in dose reductions of 20% (no anti-scatter grid) and 30% (15 cm air-gap), DNA double-strand break reductions of 30% (no anti-scatter grid) and 20% (15 cm air-gap) and a reduction of radiation-induced cancer mortality risk of up to 45%.

Conclusion: Radiation doses received during paediatric cardiac catheterisation procedures resulted in a significant increase in DNA damage while maintaining acceptable image quality and diagnostic efficacy. It is feasible to remove the anti-scatter grid resulting in a reduction in DNA damage to the patient. The γH2AX assay may be used for assessment of dose optimisation strategies in children.

Introduction

The number of paediatric cardiac catheterisation procedures has continued to increase over the last decade[1] due to their value in diagnosing and in particular, treating congenital heart disease. Unfortunately paediatric cardiac catheterisation contribute a significant radiation burden to children who are 2 - 10 times more sensitive to radiation-induced cancer compared

to adults[2-3]. The largest dosimetry study for paediatric cardiac catheterisation in the United Kingdom, consisted of >10,000 procedures and demonstrated that almost 50% of children had received radiation doses comparable to having >500 chest radiographs[4]. The lifetime risk of developing any cancer for children in receipt of numerous medical imaging examinations for congenital heart disease has been reported to be as high as 6.5%[5]. Newer flat panel detectors are thought to be more dose efficient because they are more efficient at converting X-ray photon energy into a corresponding electrical signal[6]. Determining the optimal method of imaging using flat panel detectors technology is necessary to minimise radiation dose. Simultaneously, it is important to maintain appropriate image quality in accordance with "as low as reasonably achievable" principle[7], given that there are no official imaging guidelines in this area. This has led to inconsistent imaging protocols in clinical practice[8]. The successful reduction in radiation dose for children is a priority according to the "Image Gently" campaign and the World Health Organisation[9].

The anti-scatter grid is used to absorb scattered radiation, which degrades image quality. Employing an anti-scatter grid is common practice in paediatric cardiac catheterisation, however some imaging centres remove the anti-scatter grid for children <10 kg[5,10-11] because smaller patients are associated with the production of less scatter radiation. Evidence based on experiments and simulations on polymethyl methacrylate phantoms that have also shown dose reductions up to 50%[10,12-13]. Recently one publication stated that they have begun removing the anti-scatter grid in children up to 20 kg but did not state if the anti-scatter needed to be reinserted for any of their examinations[14]. Another possible method of scatter removal is to remove the anti-scatter grid and employ an air-gap between the patient and the X-ray detector. A 15 cm air-gap has been successfully implemented on 122 adult patients undergoing cardiac

catheterisations with reported dose reductions of 23 - 39%[15]. The air-gap method has also been successfully employed in children <20 kg for cardiac biopsies[16].

To determine if radiation dose optimisation is achievable measurements of radiation dose and image quality are required. Additionally the lifetime attributable risk (LAR) of cancer mortality from radiation exposure can also be obtained. At present the linear no-threshold model is accepted by the International Commission on Radiological Protection (ICRP)[17] and assumes that a linear risk is associated with medical radiation doses, typically <100 mSv. Biomarkers of radiation exposure may also be used to assess the cellular effects of radiation exposure and have been encouraged by the United Nations Scientific Committee on the Effects of Atomic Radiation[18]. In particular the highly sensitive γH2AX assay has enabled the immunofluorescence of radiation-induced DNA double-strand breaks following *ex vivo* ionising radiation in isolated blood lymphocytes[19-23]. One of the earliest responses is the phosphorylation of the histone H2AX at serine 139[24]. The rapid accumulation of γH2AX-foci surrounding a double-strand breakage damage site enables a 1:1 assessment of the number of double-strand breakages[25]. Recently, authors have used the γH2AX assay to detect double-strand breakages in children following computed tomography[26-27] and paediatric cardiac catheterisation[28]. However, no study has been published which investigates if DNA integrity may be maintained by optimising radiation dose during these types of clinical procedure.

This will be the first study to employ the γH2AX assay a biomarker of radiation dose reduction during cardiac catheterisation procedures. The purpose of our study was to conduct a trial in paediatric cardiac catheterisation implementing either: (i) an anti-scatter grid (current departmental protocol), (ii) no anti-scatter grid or, (iii) no anti-scatter grid and the introduction of a 15 cm air-gap. These imaging methods were assessed for effects upon radiation dose, image quality, LAR of cancer mortality and DNA integrity using the γH2AX assay.

Materials and methods

Study population

The study complied with the Declaration of Helsinki[29]. Upon local governance and ethical approval (Ref: 13020CH-AS, Ref: 13/NI/0204), written informed consent was obtained from 70 consecutive participants aged 0 - 16 years (or their guardians/parents) undergoing paediatric cardiac catheterisation in a UK paediatric cardiology centre from 1st April 2014 to 31st March 2015. Participants were randomly assigned using a sealed envelope to 1 of the 3 imaging methods. Inclusion criteria were; written informed consent and aged ≤ 16 years. Parental consent was obtained from the parent/guardian of the child and if possible, the child provided assent. Exclusion criteria were; those unwilling or unable to provide consent, withdrawal from participation and emergency referrals. A second set of exclusion criteria for blood sample collection was as follows: known cancer, history of radiotherapy or chemotherapy, current viral infections, white blood cell disorders e.g. Lymphocytopenia, exposure to toxins, history of antioxidant supplementation and physical exercise two hours prior to participation.

Imaging

Imaging was performed using a Philips Allura Xper bi-plane flat panel detector cardiovascular system (Philips healthcare, Amsterdam, Netherlands) that employed an automatic exposure control. Participants were imaged using the "paediatric" setting using 15 pulses per second for fluoroscopy and 30 acquisitions per second for CINE acquisition. The X-ray system employed tube energies in the range of 60 - 100 kVp (anti-scatter grid mean 71± s.d. 3.4, No anti-scatter grid mean 68± s.d. 4.2, 15 cm air-gap mean 67± s.d. 4). Pre-set additional filtration of 0.1 mm aluminum 0.4 mm copper for fluoroscopy and 0.1 mm aluminum, 0.1 mm copper during CINE acquisition was used. No magnification was required and standard collimation was employed

throughout. Clinicians were made aware of the randomly implemented imaging method (anti-scatter grid, no anti-scatter grid or 15 cm air-gap) and had the option of reverting to the standard protocol if necessary by reinserting the anti-scatter grid. In order to remove the grid a safety catch is depressed and the grid is easily removed from the equipment or re-inserted if required, as illustrated in Figure 1.

Image quality assessment

The clinician performing the procedure continuously assessed image quality during each procedure ensuring that diagnostic efficacy was maintained. To score image quality without potential bias, and permit time to assess on image quality, retrospective blinded scoring was performed by two paediatric cardiologists using the Digital Imaging and Communications in Medicine images from random procedures. The researcher ensured that images were available from participants who received the highest and lowest radiation dose in the form of dose area product for each imaging method from 0 - 20 kg, 20 - 40 kg and >40 kg weight categories. Due to insufficient study numbers only 1 participant was assessed for the >40 kg for the no anti-scatter grid method. A 5-point Likert style scoring scale was used to assess image quality as used previously related clinical assessments including cardiac catheterisation and neonatal chest imaging[15,30]. The image characteristics assessed were based upon normal clinical considerations as follows: demonstration of the area of interest, image contrast, image sharpness, visualisation of devices/catheters/balloons and overall quality. These were scored as follows: 2 Fully confident criterion is fulfilled, 1 Somewhat confident criterion is fulfilled, 0 Uncertain whether criterion is fulfilled, -1 Somewhat confident criterion is not fulfilled, -2 Fully confident that criterion is not fulfilled.

Dosimetry

The dose area product, tube current, tube potential, field of view, focus to image distance, number of CINE acquisitions, fluoroscopy time and imaging angles were recorded in order to estimate the effective dose. Effective dose is defined by the ICRP. It is the tissue-weighted sum of the equivalent doses in all specified tissues and organs of the human body and represents the stochastic health risk to the whole body, which is the probability of cancer induction and genetic effects, of low levels of ionising radiation. Effective dose and organ dose were determined by the Monte Carlo software PCXMC version 2.0 (STUK, Helsinki, Finland). For all exposures made to each child the following were added to the PCXMC program: (i) *examination data,* included corresponding phantom age, height, mass, focus-image distance, image and field width by height, phantom exit-image distance, focus-image distance, focus-skin distance and beam angulation, (ii) *photon simulation,* included tube potential, X-ray tube anode angle and filtration, (iii) *input radiation dose* for CINE and fluoroscopy (fluoro) entered in the form of DAP in $mGy \cdot cm^2$. This program applied the tissue weighting factors recommended in the ICRP publication 103, 2007[31]. A crude estimation of peak skin dose was also made by dividing the dose area product by the field of view for the fluoroscopy and CINE acquisitions and adding together the skin dose for all overlapping regions of skin.

Blood dose estimation

The organ doses calculated for each participant were used to estimate the dose to the blood. This was performed by applying the dose to each organ and the weighted fraction of total blood volume present in the organ at any given time according to values presented in the ICRP publication 89[32].

Blood sample collection

Blood samples (1 ml) were collected through the secured vascular access sheath. One sample for each participant was collected prior to imaging to determine baseline numbers of γH2AX-foci and a second sample taken immediately following the procedure. Samples were immediately stored in a cool box at 4ºC to prevent double-strand break repair reported to occur after 30 minutes[24].

Lymphocyte separation

Blood samples were added to 1 ml phosphate-buffered solution and carefully layered using a pipette onto lymphocyte separation medium Histopaque 1077 (Sigma-Aldrich, Dorset, United Kingdom). Centrifugation was performed at 2,000 rpm for 30 minutes at 21ºC and stopped without the use of a brake mechanism. The lymphocyte layer was aspirated with a pipette, placed in 5 mls of phosphate-buffered solution and centrifuged at 1,070 rpm for 5 minutes. The resulting lymphocyte cell pellet was washed with phosphate-buffered solution and spotted onto superfrost plus slides (Menzel-Glaser, Thermo Fisher Inc, Braunschweig, Germany) and left to dry for 30 minutes. Cells were then fixed with 2% formaldehyde for 10 minutes.

Immunofluorescence and microscopy

Fixed cells were permeabilised using 0.5% Triton-X100 phosphate-buffered solution for 10 minutes and blocked in 5% horse serum and 0.1% Triton-X100 phosphate-buffered solution for 30 minutes. Cells were incubated with 1:1000 mouse anti-H2AX phosphorylated monoclonal antiphospho-histone H2AX (ser 139) clone (Millipore, Herfortshire) in the dark for one hour at room temperature followed by Alexa Fluor 488 goat anti-mouse IgG, IgA and IgM (H&L) (Life technologies, Paisley, United Kingdom) in the dark for one hour at room

temperature. Slides were washed with phosphate-buffered solution between each stage and then mounted with vectashield hardset DAPI (Vector laboratories, Peterborough, United Kingdom). The numbers of γH2AX-foci were counted using an Olympus BX3 epiflurescence microscope with x63 objective. Due to the dispersal of irradiated lymphocytes in the blood circulation 300 lymphocyte cells were scored for each sample.

***Ex vivo* irradiation**

An *ex vivo* radiation dose response calibration was performed using 7 ml whole blood obtained from the antecubital vein of a healthy volunteer. This blood sample was pipetted into 7 x 1 ml eppendorf tubes, which were irradiated to one of the following radiation doses respectively: 0 mGy, 2.5 mGy, 5 mGy, 10 mGy, 15 mGy, 30 mGy and 500 mGy using an X-RAD 225 cabinet (Precision X-ray Inc, North Branford, United States of America). Samples were placed in an incubator at 37ºC for 30 minutes prior to undergoing the γH2AX protocol, allowing time for DNA damage signaling[27].

Lifetime attributable risk cancer mortality estimation

In addition to calculating effective dose, PCXMC also provided the LAR of cancer mortality for each participant using effective dose using Biological Effects of Ionising radiation (BEIR) risk models[33]. Each child's age and ethnicity was inputted into the PCXMC program. LAR of cancer mortality was also estimated using a second method which involved γH2AX-foci observations. In order to perform this estimation the mean number of γH2AX-foci induced by the *in vitro* irradiation for 500 mGy was determined (mean = 5.25 foci per cell). A dose of 500 mGy was chosen because cancer mortality risk data is available for 500 mGy in the BEIR report (Biological Effects of Ionising radiation, 2006) [33]. The risk factor at 500mGy was

then scaled and used with the in vitro dose response curve performed using blood doses of 0-30 mGy to estimate the cancer mortality risk. The calculations were performed as follows; cancer risk for 500 mGy (from BEIR report [33]) divided by in vitro mean foci observation for 500 mGy (5.25) and multiplied by each participant foci observation to calculate their individual risk. For example we would estimate the LAR of cancer mortality for a 14 year old male patient with a mean number of induced γH2AX-foci of 0.046 and a LAR of 3% for 500 mGy (BEIR) as follows. We divided his cancer risk of 3% by the in vitro mean foci observation for 500 mGy (5.25) and multiplied this by the foci observation from his blood sample (0.046). i.e. 3/5.25x0.046 = 0.03% Therefore his LAR of cancer mortality was calculated as 0.03%.

Statistical analysis

Statistical Package for Social Science 22 (SPSS Inc, Chicago, IL, USA) was used to assess the relevant data. Pre paediatric cardiac catheterisation procedure baseline samples between participants were evaluated using a one-way ANOVA with Tukey post hoc tests. Differences in radiation dose, image quality scores, mean γH2AX-foci and LAR of cancer mortality for each imaging method were analysed using descriptive statistics. Differences between pre and post radiation γH2AX-foci observations were evaluated using the paired sample Wilcoxon signed-rank test. A Spearman's correlation coefficient was used to evaluate the relationship between γH2AX-foci and radiation dose, and LAR of cancer mortality and cancer mortality estimates using γH2AX-foci observations. Kappa measure of agreement was used to determine the inter-observer agreement between clinical image scorers. A Grubbs test was used to evaluate radiation dose and identify statistical outliers.

Results

Procedures

A total of 22 diagnostic and 48 interventional procedures were performed. On average participant size was similar for each imaging method (Table 1). One outlier was identified and removed from analysis during the study period. This participant received a dose area product of 6,672.4 cGycm², more than double the second largest dose area product, and had undergone an unusually complex and difficult procedure. A summary of the imaging parameters and procedure types are demonstrated in Table 2. Information on each participant size, weight and DAP values has been provided in Table 3. The tube potential used throughout the study ranged between 62 - 102 kVp. The anti-scatter grid group had the lowest mean fluoroscopy time (663±556) and the lowest total number of total CINE acquisitions (146). Compared to the anti-scatter grid group, mean tube current was 40% less for the no anti-scatter grid group and 25% less for the 15 cm anti-scatter group. The majority of examinations were interventional and mostly treated patent ductus arteriosus and atrial septal defects. The majority of X-ray beam angulations for fluoroscopy were performed in the posterior-anterior and lateral views.

Image quality

Image quality was deemed acceptable throughout all procedures and were completed without a request by the operating clinician to reinsert the anti-scatter grid. A sample image comparison of lateral CINE projections performed on participants weighting 10 - 20 kg for each image method is demonstrated in Figure 2. Kappa measure of agreement demonstrated significant correlation between the blinded image scorers (p <0.05). Image quality was regarded as sufficient when the image score was ≥0. The mode score for image quality characteristics was 2 (Fully confident that criterion is fulfilled) for each imaging method. All 3 imaging methods scored a 0 for image sharpness in participants >10 kg for the visualisation of balloons/stents/devices on at least 1 occasion. The mode score for overall image quality was 1

(good image quality, no limitations for clinical use) for each imaging method. Only 1 negative score was given throughout the scoring. This was a score of -1 (somewhat confident criterion is not fulfilled), specifying difficulty visualising a pulmonary stent in a participant weighting 52 kg using the no AS grid method during fluoroscopy in a left anterior oblique 65º, cranial 35º angulation.

Dosimetry

A summary of the radiation dose recorded for each imaging method is provided in Table 4. Compared to the anti-scatter grid group (843±870), the mean dose area product was 53% lower for the no anti-scatter grid group (396±152) and 20% lower for the 15 cm air-gap group (678±773). Similarly, the same trend was observed for effective dose, peak skin dose and organ doses. All peak skin dose estimations were considerably lower than the deterministic skin injury threshold of 2 Gy. The largest peak skin dose was observed in the outlier participant (481 mGy), whilst the second largest was observed in a participant imaged using the anti-scatter grid method (275.6 mGy).

Assessment of DNA double-strand breakages

One participant did not consent for a blood sample to be taken therefore the γH2AX assay was performed on 69 of the 70 participants. No significant difference was found between numbers of γH2AX-foci in the pre samples (p >0.05). An increase in γH2AX-foci was observed in each participant who underwent paediatric cardiac catheterisation. Pre radiation mean γH2AX-foci values ranged from 0 - 0.07 (up to 22/300 double-strand breakages) whilst mean post radiation γH2AX-foci ranged from 0.006 - 0.41 (up to 118 radiation-induced double-strand breakages from 300 cells). The mean numbers of radiation-induced γH2AX-foci for each imaging method are demonstrated in Figure 3. The Wilcoxin signed-rank test showed a significant

increase in γH2AX-foci following paediatric cardiac catheterisation for 84% of participants (p <0.05). The lowest radiation dose that led to a significant increase in γH2AX-foci (0.02) was observed in a 1-year-old who received a dose area product of 81 cGycm² using the anti-scatter grid for a diagnostic procedure. The largest mean increase in γH2AX-foci (0.35) was observed in an 8-year-old who received a dose area product of 2,617.4 cGycm² using the anti-scatter grid method for a diagnostic assessment of previous intervention for tetralogy of fallot. Compared to the mean number of radiation-induced γH2AX-foci using the anti-scatter grid method (0.1±0.08) mean γH2AX-foci were 30% and 20% lower for the no anti-scatter grid (0.07±0.06) and 15 cm air-gap (0.08±0.07) methods respectively. Almost all participants imaged with the anti-scatter grid (96%) had significant increases in mean γH2AX-foci beyond their background (pre) level, whilst for the no anti-scatter grid (77%) and 15 cm air-gap (83%) this figure was lower.

Lifetime attributable risk of cancer mortality

The in vitro dose response curve performed using lower blood doses of 0-30 mGy and the number of radiation-induced γH2AX-foci for each participant (Figure 4) was used to estimate a cancer mortality risk for each participant. The LAR of cancer mortality for participants is demonstrated in Table 5. Estimates using the biological effects of ionising radiation ranged from 0.03 - 4.8 per 1,000 (mean 0.09 per 1,000). When compared to the anti-scatter grid method, LAR of cancer mortality was 18 - 45% lower for the no anti-scatter grid method and 12 - 45% lower for the 15 cm air-gap method. Pearsons correlation coefficient demonstrated a significant agreement between biological effects of ionising radiation estimates and γH2AX-foci risk estimates (p <0.05). These observations showed that γH2AX-foci, as a measure of DNA double-strand breakages, when compared with the PCXMC BEIR estimates

demonstrated an agreement with the linear no-threshold model of radiation-induced cancer risk estimates for < 500 mGy.

Discussion

This is the first study to use biomarker evidence following implementation of dose optimisation in paediatric cardiac catheterisation. The data presented is the largest known study to assess double-strand breakages as a result of ionising radiation exposure to children, and from paediatric cardiac catheterisation procedures. Children that received a dose area product as low as 81 cGycm² resulted in significant amounts of double strand breakages; the most significant DNA lesions induced by ionising radiation. Although these double-strand breakages were undergoing repair, there is an increased risk of a non-repair or misrepair event, potentially leading to carcinogenesis[34]. Our baseline levels of double-strand breakages were within the region expected for non-irradiated blood lymphocyte cells (<0.1)[35-36]. We used our *ex vivo* double-strand breakage observations to interpret the *in vivo* findings. Although our *in vivo* correlation between foci and blood dose was weaker than *ex vivo*, likely because of repair already occurring during paediatric cardiac catheterisation, an increase in double-strand breakages clearly occurred with increasing radiation dose to participants. The no anti-scatter grid method and the consequent reduction in radiation dose, resulted in an average reduction in DNA damage of 30%, whilst for the 15 cm air-gap, the average reduction was 20%. The observed amounts of DNA damage repair are in general agreement with previous *in vivo* investigations in children undergoing medical imaging[26-28]. Almost all participants imaged with the anti-scatter grid (96%) had significant increases in mean γH2AX-foci beyond their background (pre) level, whilst for the no anti-scatter grid (77%) and 15 cm air-gap (83%) this figure was lower. This would indicate that 23% and 17% of participants undergoing the

proposed optimisation techniques maintained DNA integrity at pre intervention levels at these radiation doses.

The estimated LAR of cancer mortality used biological effects of ionising radiation risk models took into consideration the age and gender of the participants. The linear no-threshold model assumes that there is no safe amount of ionising radiation and therefore all exposures no matter how low, carry some risk. The range of percentage LAR of cancer mortality reported in males (0.02 - 0.53) and females (0.011 - 0.53) from previous investigation[26] resemble the range of estimates found in our study using the anti-scatter grid method for males (0.017 - 0.48) and females (0.03 - 0.4). In comparison these were lower for the no anti-scatter grid method (males: 0.003 - 0.18, females: 0.03 - 0.24) and 15 cm air-gap method (males: 0.01 - 0.18, females: 0.004 - 0.18). We found LAR cancer mortality estimates using γH2AX-foci observations were similar to the PCXMC BEIR estimates and therefore support the current consensus of the linear no-threshold model. This finding is contrary to a previous investigation, which used γH2AX-foci observations, finding that LAR of cancer mortality using γH2AX-foci data was four times greater (4 per 1000) than biological effects of ionising radiation estimates (1 per 1000)[28].

The results of our random clinical implementation of scatter removal techniques suggest that removal of the anti-scatter grid in routine diagnostic and interventional paediatric cardiac catheterisation is feasible. The average dose reductions observed by reverting to a no anti-scatter grid method (53%) or 15 cm air-gap method (20%) also demonstrated sufficient image quality for successful completion of all paediatric cardiac catheterisation procedures in participants up to 15 years of age, 99 kg and 22 cm chest diameter. These dose reductions are

likely because the tube current for the anti-scatter grid was 40% and 25% greater than the no anti-scatter grid and 15 cm air-gap methods. This was expected because the X-ray system uses an automated exposure control to maintain a constant detector dose, therefore tube current is automatically increased using an anti-scatter grid. This occurs because useful X-ray photons are absorbed by the interspaced material positioned within the lead strips of the anti-scatter grid. It is important to note that these reductions in dose were observed in spite of an increase in fluoroscopy time and the number of acquisitions undertaken in both the group where the anti-scatter grid was removed and the group with the air gap. This implies that dose reduction was achieved by employing these techniques irrespective of the complexity of the case but may also indicate extra procedural time required to complete the examination due to reduced image quality.

Mean effective dose observations ranged from 4.55 mSv (no anti-scatter grid) to 6.78 mSv (anti-scatter grid). These observations are comparable with the range observed in previous dosimetry studies for paediatric cardiac catheterisation[4,37-39]. The greatest internal organ radiation doses occurred to the heart and lungs and on average were lower when the anti-scatter grid was removed. Regardless of the imaging method, observed organ doses were substantially below the 500 mGy dose, whereby evidence of radiation-induced cardiovascular disease exists[40]. Although only approximated, peak skin dose observations were considerably lower than the deterministic threshold of 2 Gy. These findings are consistent with previous findings that patients <18 years of age have considerably lower risk of skin injury compared to adults[41]. However it should be acknowledged that the average age in our study was five years. It could be useful further assess peak skin dose because published dosimetry observations have shown a marked increase in radiation doses for children >10 years[4,34].

Our findings are comparable with previous phantom experiments[10,13], whereby image quality was deemed sufficient for small children (<10 kg). The results also support the suggestion[12] that the anti-scatter grid may be removed for larger patients (>10 kg). Supplementary image quality scoring helped operating clinicians reflect upon a random sample of images used for each imaging method. Interestingly, all three imaging methods showed moderate lack of image sharpness for the visualisation of balloons/stents/devices on at least one occasion. This indicates that image quality could be comparable and that perhaps temporarily increasing the detector dose could remedy this problem. Our X-ray system enables the selection "fluoro flavours" that may boost image quality (at the expense of increasing the radiation dose) for a brief period. The negative score for the visualisation of a pulmonary stent in a large participant using the no anti-scatter grid method during fluoroscopy with a steep imaging angle, has identified potential scenario justifying the use of the anti-scatter grid.

The use of automatic exposure control flat panel detector imaging systems without an anti-scatter grid *in situ* substantially lowers radiation dose to the patient. Less scatter radiation occurs when imaging smaller patients and a lower tube output by removing the anti-scatter grid will also inevitably result in less scatter radiation. Our study has shown, that during paediatric cardiac catheterisation, the amounts of scatter radiation in newborns and small children up to approximately 20 kg may be insufficient to degrade the task dependant image quality in a range of typical paediatric cardiac catheterisation procedures. This may also be applicable to larger children but requires further evaluation. The use of the 15 cm air-gap was also used as a dose optimised method and could be useful for larger children.

Limitations

Recruited during the 1-year period was restricted to 1 - 3 per week because the departmental workload consisted mostly of adult patients. Only one imaging centre was used in the data collection whilst operating clinicians in other centres may have a different opinion on the task dependant image quality. Other imaging centres may have different X-ray beam angulation preferences and this may affect image quality differently. The radiation dose measurements calculated in our study are best estimates only. The fundamental measurement of radiation exposure was the dose area product, which as a measurement, does not reflect the amount of radiation absorbed by each participant. Monte Carlo software conversion factors were used to provide effective dose estimates however these methods provide crude estimates and have inherent inaccuracies of up to 40% [31]. There was also potential inaccuracy calculating effective and organ doses because assigning patients to the closest phantom age can result in errors as large as 25%[42]. It is important to emphasise that the observed double-strand breakages were undergoing repair and that we did not determine if full repair of double-strand breakages occurred. It is possible DNA damage observations did not capture all double-strand breakages because paediatric cardiac catheterisation is a lengthy procedure and the optimal time of capture for double-strand breakages is 30 minutes post irradiation[43]. The DNA damage observed was limited to blood lymphocytes and therefore the biological effects has not assessed the amount of DNA damage in regions such as the bone marrow, lung and breasts. It is also not possible to determine how many lymphocytes within the sample obtained were directly exposed to radiation during the procedure.

Future consideration

There are no official guidelines for best clinical practice in paediatric cardiac catheterisation. Our findings require further validation on a larger cohort due to the wide variation in patient size, types of congenital heart disease, imaging angulations and procedural complexity

associated with paediatric cardiac catheterisation. Consideration could be given to adapting other components such as "fluoro flavours" temporarily during the procedure rather than use of the anti-scatter grid. Innovation of remote control instantaneous anti-scatter grid placement and removal could also be employed in similar fashion. Investigations using the γH2AX assay have demonstrated significant reductions in radiation-induced double-strand breakages in blood lymphocytes irradiated *in vitro* with 10 mGy following oral ingestion of antioxidants[44-45]. Therefore the potential protective measure of antioxidant supplementation should be further investigated in paediatric cardiac catheterisation. Obtaining blood samples post 24 hours from paediatric cardiac catheterisation may also help identify persistent double-strand breakages.

Conclusion

This is the first study to employ the γH2AX assay a biomarker of radiation dose reduction during alterations to cardiac catheterisation procedures. Radiation doses received during paediatric cardiac catheterisation procedures resulted in a significant increase in DNA damage. Our study suggests it is feasible to implement removal of the anti-scatter grid in paediatric cardiac catheterisation to optimise the radiation dose and maintain DNA integrity. Interestingly DNA integrity was maintained in 23% and 17% of cases which may be due to ongoing DNA repair. However, caution should be given to larger children for employing balloon/stent/devices, whereby the use of a 15 cm air-gap may be preferable. Our findings showed acceptable image quality and substantial reductions in radiation dose. Consequently, a substantial reduction in DNA damage and cancer mortality risk has been presented. Based upon our work, a larger investigation is warranted and we hope that presented material will further the knowledge for clinicians making risk-benefit decisions during imaging for paediatric cardiac catheterisation.

Conflict of Interest

On behalf of all authors, the corresponding author states that there is no conflict of interest.

References

1. Harbron, RW, Pearce, MS, Salotti, JA et al. Radiation doses from fluoroscopically guided cardiac catheterisation procedures in children and young adults in the United Kingdom: a multicentre study. Br J Radiol, 2015; 88 (1048), 20140852.

2. United Nations. Scientific Committee on the Effects of Atomic Radiation. Sources and effects of ionising radiation: Sources. Vol 1. United Nations Publications; 2000.

3. Rassow J, Schmaltz A, Hentrich F, Streffer C. Effective doses to patients from paediatric cardiac catheterisation. Br J Radiol. 2000;73(866):172-183.

4. Harbron RW, Pearce MS, Salotti JA et al. Radiation doses from fluoroscopically guided cardiac catheterisation procedures in children and young adults in the United Kingdom: a multicentre study. The Br J Radiol. 2015; 88 (1048), 20140852.

5. Johnson, JN, Hornik CP, Li JS et al. Cumulative radiation exposure and cancer risk estimation in children with heart disease. Circulation. 2015; 130 (2), 161-167.

6. Seibert, J.A. 2006. Flat-panel detectors: how much better are they? Pediatr Radiol, 36 (2) 173-181.

7. Strauss KJ, Sue CK. “The ALARA (as Low as Reasonably Achievable) Concept in Paediatric Interventional and Fluoroscopic Imaging: Striving to Keep Radiation Doses as Low as Possible during Fluoroscopy of Paediatric Patients—a White Paper Executive Summary.” Pediatr Radiol. 2015; 36.Suppl 2 (2006): 110 - 112.

8. McFadden, S., Hughes, C, Winder, R. Variation in radiographic protocols in paediatric interventional cardiology. J Radiol Prot. 2013; 33 (2), 313.

9. Goske MJ, Applegate KE, Bulas D et al. Image gently: Progress and challenges in CT education and advocacy. Pediatr Radiol. 2011;41(2):461- 466.

10. McFadden SL., Hughes CM., Mooney RB, Winder RJ. An analysis of radiation dose reduction in paediatric interventional cardiology by altering frame rate and use of the anti-scatter grid. J Radiol Prot. 2013; 33 433-443.

11. Ghelani SJ, Glatz AC, David S et al. Radiation Dose Benchmarks During Cardiac Catheterisation for Congenital Heart Disease in the United States. JACC Cardiovasc Interv. 2014; 7 (9), 1060-1069.

12. Gislason AJ, Davies AG, Cowen AR. Dose optimization in paediatric cardiac x-ray imaging. Medical physics. 2010; 37 5258.

13. Ubeda, C., Vano, E., Gonzalez, L, Miranda, P. Influence of the antiscatter grid on dose and image quality in paediatric interventional cardiology X□ray systems. Catheter Cardiovasc Interv. 2013; 82 (1), 51-57.

14. Mauriello, D.A., Fetterly, K.A., Lennon, R.J et al. Radiation reduction in paediatric and adult congenital patients during cardiac catheterisation. Catheter Cardiovasc Interv. 2014; 84 (5), 801–808.

15. Partridge, J., McGahan, G., Causton, S et al. Radiation dose reduction without compromise of image quality in cardiac angiography and intervention with the use of a flat panel detector without an antiscatter grid. Heart. 2006 92 (4), 507-510.

16. Sutton, N.J., Lamour, J., Gellis, L.A, Pass, R.H. Paediatric patient radiation dosage during endomyocardial biopsies and right heart catheterisation using a standard "ALARA" radiation reduction protocol in the modern fluoroscopic era. Catheter Cardiovasc Interv. 2014; 83 (1), 80-83.

17. International Commission on Radiological Protection (ICRP), 2005. Low-dose Extrapolation of Radiation-related Cancer Risk. ICRP Publication 99. Ann. ICRP 35 (4).

18. United Nations Scientific Committee on the Effects of Atomic Radiation (UNSCEAR). Sources, effects and risks of ionising radiation. 2013; (II).New York: UNSCEAR.

19. Rothkamm, K., Krüger, I., Thompson, L.H, Löbrich, M. Pathways of DNA double-strand break repair during the mammalian cell cycle. Molecular and cellular biology. 2003; 23 (16), 5706-5715.

20. Rothkamm, K, Lobrich, M. Evidence for a lack of DNA double-strand break repair in human cells exposed to very low x-ray doses. Proc Natl Acad Sci U S A. 2003 100 (9), 5057-5062.

21. Kühne, M., Riballo, E., Rief, N., Rothkamm, K., Jeggo, P.A, Lobrich, M. A double-strand break repair defect in ATM-deficient cells contributes to radiosensitivity. Cancer research. 2004; 64 (2), 500-508.

22. Riballo, E., Kühne, M., Rief, N. A pathway of double-strand break rejoining dependent upon ATM, Artemis, and proteins locating to γ-H2AX foci. Molecular cell. 2004 16 (5), 715-724.

23. Gould, R., Horn, S., Prise, K.M., Doyle, P, Hughes, C.M. Assessment of DNA double-strand breaks induced by intravascular iodinated contrast media following in vitro irradiation and in vivo paediatric cardiac catheterisation. Contrast Media Mol Imaging. 2015; Available from: http://dx.doi.org/10.1002/cmmi.1671.

24. Roch-Lefevre, S., Mandina, T., Voisin, P et al. Quantification of gamma-H2AX foci in human lymphocytes: a method for biological dosimetry after ionising radiation exposure. Radiation research. 2010; 174 (2), 185-194.

25. Jeggo, P.A, Lobrich, M. DNA double-strand breaks: their cellular and clinical impact? Oncogene. 2007; 26 (56), 7717-7719.

26. Halm, B.M., Franke, A.A., Lai, J.F et al. γ-H2AX foci are increased in lymphocytes in vivo in young children 1 h after very low-dose X-irradiation: a pilot study. Pediatr Radiol. 2014; 44 (10), 1310-1317.

27. Vandevoorde, C., Franck, C., Bacher, K et al. γ-H2AX foci as in vivo effect biomarker in children emphasize the importance to minimize x-ray doses in paediatric CT imaging. Eur Radiol. 2014; 25 (3), 800-811.

28. Beels, L., Bacher, K., De Wolf, D., Werbrouck, J. and Thierens, H. gamma-H2AX foci as a biomarker for patient X-ray exposure in paediatric cardiac catheterisation: are we underestimating radiation risks? Circulation. 2009; 120 (19), 1903-1909.

29. World Medical Association. "Declaration of Helsinki: Ethical Principles for Medical Research Involving Human Subjects". JAMA. 2013 310 (20): 2191–2194. Available at doi:10.1001/jama.2013.281053. PMID 24141714. Retrieved July 24, 2015.

30. Dougeni, E., Delis, H., Karatza, A et al. Dose and image quality optimization in neonatal radiography. The Br J Radiol. 2007; 80(958), pp. 807–815.

31. International Commission on Radiological Protection (ICRP). ICRP publication 103: The 2007 recommendations of the ICRP. Annals of the ICRP. 2007; 37 (2-4).

32. Valentin, J. Basic anatomical and physiological data for use in radiological protection: reference values: ICRP Publication 89. Annals of the ICRP. 2002; 32 (3), 1-277.

33. BEIR, V. Committee to Assess Health Risks from Exposure to Low Levels of Ionising Radiation, National Research Council. Health Risks from Exposure to Low Levels of Ionising Radiation: BEIR VII–Phase 2. 2006.

34. Verghese, G.R., McElhinney, D.B., Strauss, K.J. and Bergersen, L. Characterization of radiation exposure and effect of a radiation monitoring policy in a large volume paediatric cardiac catheterisation lab. Catheter Cardiovasc Interv. 2012; 79 (2), 294-301.

35. Rothkamm, K., Balroop, S., Shekhdar, J., Fernie, P. and Goh, V. Leukocyte DNA damage after multi-detector row CT: a quantitative biomarker of low-level radiation exposure. Radiology. 2007; 242 (1), 244-251.

36. Rothkamm, K, Horn, S. gamma-H2AX as protein biomarker for radiation exposure. Ann Ist Super Sanita. 2009; 45 (3), 265-271.

37. Yakoumakis, E., Gialousis, G., Papadopoulou, D et al. Estimation of children's radiation dose from cardiac catheterisations, performed for the diagnosis or the treatment of a congenital heart disease using TLD dosimetry and Monte Carlo simulation. J Radiol Prot. 2009; 29 (2), 251.

38. Barnaoui, S., Rehel, J., Baysson, H et al. Local reference levels and organ doses from paediatric cardiac interventional procedures. Pediatr Cardiol. 2014; 35 (6), 1037-1045.

39. Glatz, A.C., Patel, A., Zhu, X et al. Patient Radiation Exposure in a Modern, Large-Volume, Paediatric Cardiac Catheterisation Laboratory. Pediatr Cardiol. 2014; 1-9.

40. International Commission on Radiological Protection (ICRP). Cousins C., Miller D.L., Bernardi G et al. ICRP publication 120. Radiological Protection in Cardiology. Annals of the ICRP. 2012; 42(1).

41. Sawdy, J.M., Kempton, T.M., Olshove, V et al. Use of a dose□dependent follow□up protocol and mechanisms to reduce patients and staff radiation exposure in congenital and structural interventions. Catheter Cardiovasc Interv. 2011; 78 (1), 136-142.

42. Bacher, K., Bogaert, E., Lapere, R., De Wolf, D, Thierens, H. Patient-specific dose and radiation risk estimation in paediatric cardiac catheterisation. Circulation. 2005 111 (1), 83-89.

43. Horn, S., Barnard, S, Rothkamm, K. (2011). Gamma-H2AX-Based Dose Estimation for Whole and Partial Body Radiation Exposure. PLoS ONE. 2011; 6(9), e25113. doi:10.1371/journal.pone.0025113

44. Kuefner, M.A., Brand, M., Ehrlich, J., Braga, L., Uder, M. and Semelka, R.C. Effect of antioxidants on x-ray–induced γ-H2AX foci in human blood lymphocytes: preliminary observations. Radiology. 2012; 264 (1), 59-67.

45. Brand, M., Sommer, M., Ellmann, S et al. Influence of Different Antioxidants on X-Ray Induced DNA Double-Strand Breaks (DSBs) Using γ-H2AX Immunofluorescence Microscopy

in a Preliminary Study. PloS one. 2015; 10(5). Available from: http://www.ncbi.nlm.nih.gov/pmc/articles/PMC4440758/.

Figure 1 equipment with grid in situ (a) and following removal of the grid by depressing the safety catch (b).

(a)  (b) 

Figure 2. Lateral CINE image frames for assessment of patent ductus arteriosus in 10 - 20 kg participants for each imaging method

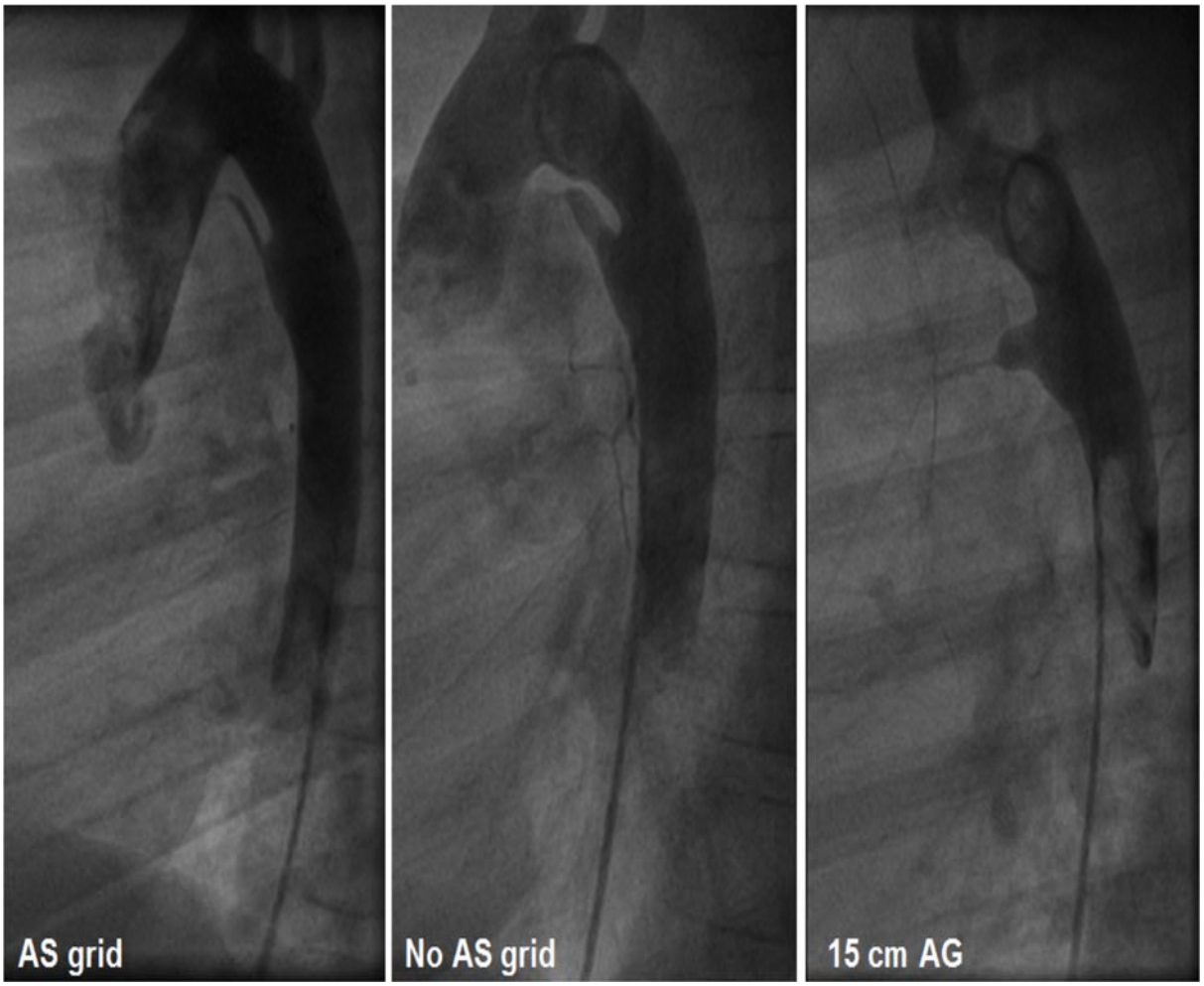
AS grid
No AS grid
15 cm AG

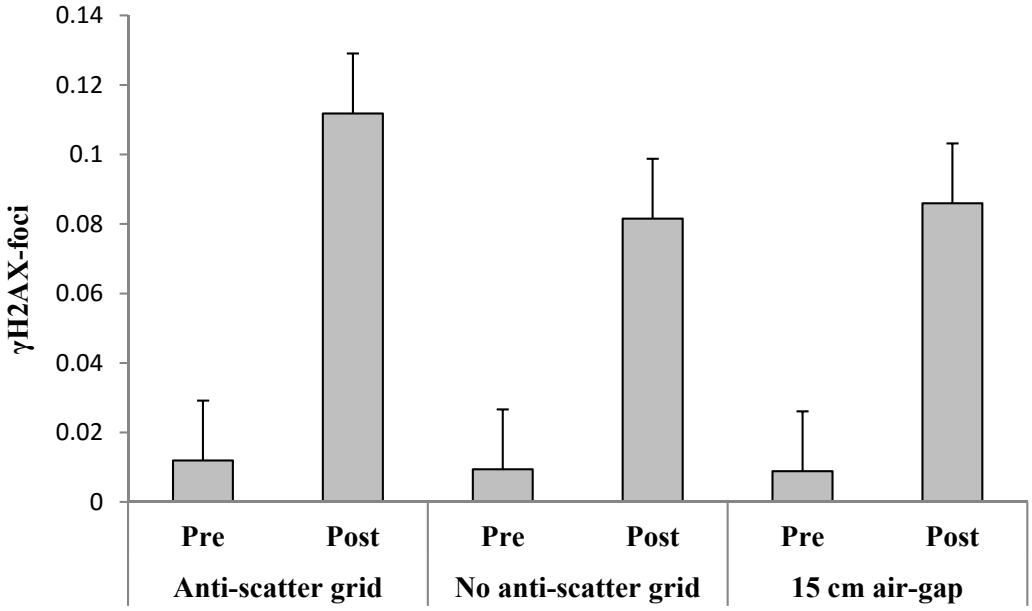

Figure 3. Mean and standard deviation of pre and post γH2AX-foci observations for each imaging method

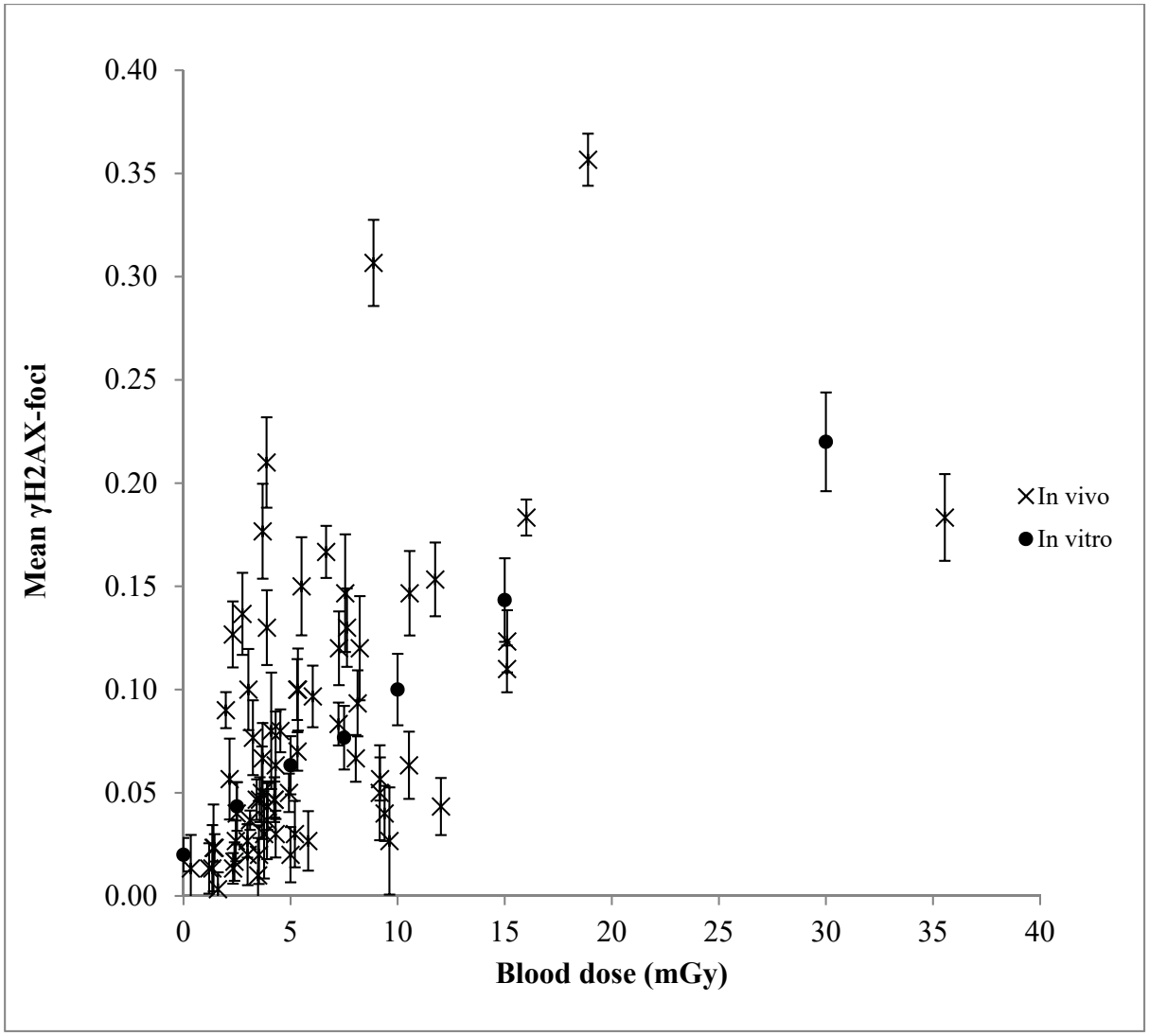

Figure 4. Mean and standard error for *in vivo* γH2AX-foci observations for all 69 participants and *in vitro* observation in a health volunteer.

Table 1. Summary of participant characteristics

	Anti-scatter grid	No anti-scatter grid	15 cm air-gap
Patients (n)	24	23	23
Males (n)	12	13	12
Females (n)	12	13	11
*Age (months)	70.7±58.2	63.3±42.3	77.2±53.4
*Weight (kg)	23±16	20.1±12	24.8±21.1
*Chest diameter (cm)	12.9±2.8	12.4±1.8	12.7±3.1

* *data presented as mean and +/- standard deviation*

Chest diameter measured using callipers

Table 2. Summary of X-ray parameters and examination types.

	Anti-scatter grid	No anti-scatter grid	15 cm air-gap
*Fluoroscopy time (s)	663±556	813±633	843±573
*Tube potential (kVp)	71±3.4	68±4.2	67±4
*Tube current (mA)	357±214	216±93	267±163
*CINE time (s)	4.3±1.4	4.3±1.3	4.1±2.1
Total CINE acquisitions (n)	146	177	151
Diagnostic (n)	5	8	9
Patent ductus arteriosus (n)	10	9	5
Atrial septal defect (n)	3	1	6
Pulmonary valve stenosis (n)	2	1	0
Aortic valve stenosis (n)	1	1	1
Aortic stenosis	1	0	0
Pulmonary artery stenosis (n)	2	1	1
Permanent pacemaker (n)	0	1	1

** Data presented as mean and +/- standard deviation*

Table 3. Patient size, weight and DAP values.

Imaging method	Age (months)	Weight (kg)	Height (cm)	Chest thickness (cm)	DAP (cGycm²)
Anti-scatter grid	96	27.2	129.3	13.5	2617.4
Anti-scatter grid	16	7.86	70	10.5	266.3
Anti-scatter grid	61	14	101.5	13	545.1
Anti-scatter grid	2	4.95	57.5	9	121.3
Anti-scatter grid	105	34	147	11	463.4
Anti-scatter grid	101	31	129	14	1079.4
Anti-scatter grid	19	11.15	80.5	12	81.4
Anti-scatter grid	17	12	85.5	9	199.8
Anti-scatter grid	19	10.76	86	10.5	162.7
Anti-scatter grid	34	13.42	88.8	11	212.8
Anti-scatter grid	6	7.8	70	11	140.8
Anti-scatter grid	0	3.3	51	8.5	34
Anti-scatter grid	40	13.4	95	12.5	2836.9
Anti-scatter grid	99	30	126	15	1092.9
Anti-scatter grid	23	10.6	75	12	213.1
Anti-scatter grid	72	22.5	121.1	15	349.9
Anti-scatter grid	171	40	159	16.5	880
Anti-scatter grid	162	51	165	17	2529.8
Anti-scatter grid	138	53	159.5	19	585
Anti-scatter grid	43	16.1	94.5	12.5	266.8
Anti-scatter grid	173	44	158.5	17	1447.6
Anti-scatter grid	178	59	162	17	958.2
Anti-scatter grid	46	15	102	12	814.2
Anti-scatter grid	78	22	117	13	2330
No anti-scatter grid	29	11.5	87	11.00	211.8
No anti-scatter grid	156	46	157	15.50	308.7
No anti-scatter grid	106	38.7	146.3	14.00	4.34
No anti-scatter grid	8	6.2	67	8.50	115.7
No anti-scatter grid	133	32	139.6	15.50	648.9
No anti-scatter grid	60	17.5	109	13.00	342
No anti-scatter grid	138	52	147.5	16.00	6672.4
No anti-scatter grid	84	16.54	107.5	11.50	481.1
No anti-scatter grid	49	18.62	108.1	11.2	157.6
No anti-scatter grid	63	18	102	10.2	764.3
No anti-scatter grid	16	9.25	85	11	101.2
No anti-scatter grid	11	9	75	11	129.8
No anti-scatter grid	73	17	109.5	12.5	196.6
No anti-scatter grid	96	26	124.4	14	970.5

No anti-scatter grid	62	16.5	107.5	12	164.7
No anti-scatter grid	32	13.5	97	11.5	380.9
No anti-scatter grid	39	14.95	93	12.5	266.5
No anti-scatter grid	51	17.65	11	14	925.8
No anti-scatter grid	58	14.5	106	12.8	1418.4
No anti-scatter grid	6	6	67	11	315.4
No anti-scatter grid	20	11.5	86.5	11	92
No anti-scatter grid	63	24.85	114	13	504
No anti-scatter grid	104	26	115	12	216.9
15 cm air-gap	168	57	172	17	998.6
15 cm air-gap	39	14.55	92.5	12	1240.2
15 cm air-gap	56	18.4	108	11.5	790.4
15 cm air-gap	100	24	130	13.5	262.7
15 cm air-gap	51	17.1	100.5	11.5	825.8
15 cm air-gap	48	16	101	12	338.7
15 cm air-gap	90	21	119.5	11	697
15 cm air-gap	140	25	121.5	12.5	27.8
15 cm air-gap	68	23.5	110	13	374.1
15 cm air-gap	8	8.05	70	9	393.4
15 cm air-gap	183	99	170	18.5	2755.4
15 cm air-gap	51	14	94	11	154.4
15 cm air-gap	36	12.38	85	11.5	367.9
15 cm air-gap	24	11.2	82	10.5	134.8
15 cm air-gap	75	16.85	90	13.5	226
15 cm air-gap	6	7.3	68	10	162.2
15 cm air-gap	42	11.3	98	8	88.6
15 cm air-gap	54	16.35	102	13	886
15 cm air-gap	22	10.5	80	10	330.3
15 cm air-gap	107	32	143	17	171
15 cm air-gap	87	22.2	108	12	221.7
15 cm air-gap	132	32.5	148	13	1191.3
15 cm air-gap	190	61	164	22	2946.5

Table 4. Summary of mean and standard deviation of radiation dose estimations using each imaging method

Organ	Anti-scatter grid	No anti-scatter grid	15 cm air-gap
DAP (cGycm²)	843±870	396±352	678±774
Effective dose (mSv)	6.78±7.72	4.45±3.73	4.66±3.39
Peak skin dose (mGy)	52.2±57.9	21.5±16.5	45.6±46.2
Lung (mGy)	23.9±22.7	15.1±12.5	17.5±12.2
Heart (mGy)	18.3±18.6	10.6-7.7	12.1±7.5
Oesophagus (mGy)	16.6±18.9	9.1±6.5	11.3±8.3
Adrenal (mGy)	17.9±46.2	5.2±6.2	6.5±5.4

Table 5. Mean and standard deviation of percentage LAR of cancer mortality for males and females for each imaging method using BEIR estimates and calibrated γH2AX-foci observations.

		Anti-scatter grid	No anti-scatter grid	15 cm air-gap
Males	BEIR	0.09±0.04	0.05±0.05	0.07±0.04
	FOCI	0.09±0.06	0.06±0.04	0.08±0.07
Females	BEIR	0.11±0.1	0.09±0.06	0.09±0.06
	FOCI	0.11±0.1	0.08±0.09	0.06±0.04